Available online at www.sciencedirect.com

ScienceDirect

journal homepage: www.elsevier.com/locate/he

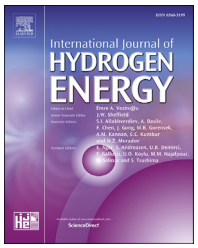

Silver cluster supported on nitrogen-doped graphene as an electrocatalyst with high activity and stability for oxygen reduction reaction

Seifollah Jalili [a,b,*], *Elham Moharramzadeh Goliaei* [a], *Jeremy Schofield* [c]

[a] *Department of Chemistry, K. N. Toosi University of Technology, P. O. Box 15875-4416, Tehran, Iran*
[b] *School of Nano-Science, Institute for Research in Fundamental Sciences (IPM), P.O. Box 19395-5531, Tehran, Iran*
[c] *Chemical Physics Theory Group, Department of Chemistry, University of Toronto, 80 Saint George Street, Toronto, Ontario, M5S 3H6, Canada*

ARTICLE INFO

Article history:
Received 19 January 2017
Received in revised form
21 April 2017
Accepted 23 April 2017
Available online 13 May 2017

Keywords:
Nitrogen-doped graphene
Ag_8 cluster
Oxygen reduction reaction
d-Band center
Bader charge analysis

ABSTRACT

An Ag_8 cluster deposited on three different types of nitrogen (N)-doped graphene was studied using density functional theory calculations with empirical pair potentials (DFT-D). Among the different kinds of N-doped graphene, the pyridinic-N_3 (P-N_3) type can act as the best anchor position to stabilize Ag_8. In addition, it is found that supported Ag_8 clusters show higher activity in oxygen reduction reaction compared to unsupported clusters due to significant decrease in O_2 adsorption energy and higher charge transfer to O_2. Electron transfer from Ag to O_2 leads to the elongation of the O–O bond, which facilitates the breaking of this bond in the oxygen reduction reaction. All results suggest that N-doped graphene support can play a significant role in the chemical reactivity of a Ag_8 cluster in oxygen reduction reaction.

Introduction

Nowadays, the production of clean energy has attracted considerable attention from the scientists. The role of fuel cells is undeniable, given their efficient performance in the production of clean energy [1–4]. In addition, the efficiency of fuel cells is dependent on electrocatalysts, which can improve the activity of the oxygen reduction reaction (ORR) [5]. Hence, the development and design of new electrocatalysts will play a fundamental role in fuel cell systems.

In the search for electrocatalysts, many studies have been conducted using precious metal catalysts, such as Pt [6–9], Pd [10,11] and non-precious metal catalysts, like Fe [12–16] and Ag [17,18] nanoparticles deposited on support, thanks to their high activity in ORR. Density functional calculation (DFT) examinations have been performed to investigate support effects on ORR activity of Pt [19–21] and Pd [22,23]. Among these efforts, adding heteroatoms (such as boron, nitrogen, phosphorous, sulfur and oxygen) [24] or defects [25] in graphene are promising ways to enhance the adhesion of metal catalysts and add to the electrochemical performance of graphene

* *Corresponding author*. Department of Chemistry, K. N. Toosi University of Technology, P. O. Box 15875-4416, Tehran, Iran. Fax: +98 21 22853650.
E-mail address: sjalili@kntu.ac.ir (S. Jalili).
http://dx.doi.org/10.1016/j.ijhydene.2017.04.238

sheets. Presenting heteroatoms and defects as anchor points can lead to an increased interaction between clusters and the graphene surface and can help prevent the aggregation of nanoparticles. The support can stabilize nanoparticles and reduce the O_2 [19] and O [20–23] adsorption energies. Recently, the use of clusters of Ag has drawn much attention due to its low-cost and resistance to poisoning [26]. During the recent years, silver nanoparticles supported on nitrogen-doped (N-doped) carbon nanotubes [27], nanosheets of reduced graphene oxide [17], Graphene [28], carbon nanotube [29], graphitic carbon nitride [30], N-doped reduced graphene oxide [31], multi-walled carbon nanotube [32] and N-doped graphene (N-doped) [33–35] have been drawn researchers' attention as the ORR catalysts. Jin and coworkers recently designed a new way to deposit Ag nanoclusters on N-doped graphene using single-stranded DNA and $AgNO_3$ [33]. They claimed that Ag cluster supported on N-doped graphene acts as an ORR electrocatalyst in alkaline media with high electrochemical stability in comparison with other electrocatalysts using other materials like Pt/C. The deposition of a Ag cluster on the N-doped graphene can lead to a maximization of the nanocatalyst surface area and give an electrocatalyst with higher catalytic performance compared to both N-doped graphene sheets and nanoclusters.

The ORR mechanism on Ag catalyst in alkaline media has been studied. In 1970, Appleby [36] argued that the rate-determining step for ORR on Ag is the adsorption of O_2 on the surface. Now, there is general agreement that the transfer of the first electron to O_2, and formation of O_2^- is the rate-determining step in ORR on Ag catalyst [37–40]. For Ag, the key ORR steps in alkaline condition can be summarized in three steps: (i) O_2 adsorption; (ii) HOO^- formation; (iii) HOO^- dissociation and OH formation. So, in the last step, the O–O bond is broken. It should be mentioned that too low adsorption energy of O_2 leads to a slow O–O bond breakage [41]. In contrast, the high adsorption energy of oxygen can assist the breaking of O–O bond, although it causes strongly-bound water oxidation products such as OH and O species [42]. So, the optimal catalyst has low O_2 adsorption energy and elongation of the O_2 bond due to a charge transfer from catalyst to O_2 facilitates the O–O bond-breaking and diminishes the stability of intermediates. Norskov and coworkers [43] have proposed a volcano-type relationship. According to this relationship, for Ag and Au the weak adsorption energies of oxygen atoms is the rate-determining step, although for Pt, Pd, Ir, Cu, Rh, Ni, Ru, Co, Fe, Mo and W the rate-determining step is the OH adsorption [2]. The authors of [44] argue that defective graphene-supported Pt nanoparticles transfer charge to O_2 which leads to a reduction in O_2 dissociation activation energy and decreasing the intermediate stability. Hence, the O_2 adsorption energy and the charge gained by O_2 act as critical factors for ORR activity on Ag metal.

Various N-doped graphene sheets including graphitic, pyridinic and pyrrolic nitrogen [45–48] have been studied for different applications such as ORR catalyst in fuel cell cathodes [49,50], catalyst in oxygen evolution reaction (OER) in lithium-air batteries [51], hydrogen evolution reaction (HER) catalyst [52] and lithium ion battery (LIB) anode [53]. Experimentally, graphite sheets with nitrogen content of 13% [54] and 18% wt [55] have been synthesized, including above-mentioned nitrogen species. Moreover, computational studies show that graphite sheets with nitrogen atom content less than 33.3% are stable [56]. Surprisingly, no detailed computational study has been conducted to examine these different types of nitrogen doping in one graphene sheet for ORR applications. However, Zhang and coworkers [57] focused on these issues and studied spin and charge density of graphitic and pyridinic nitrogen in one graphene sheet in the present of 8%, 12%, 25% and 33% nitrogen content. Their results show that the graphene sheet with 25% nitrogen atom content shows a high catalytic activity for ORR.

There are few reports on the electronic structure of Ag clusters deposited on graphene. The latest studies have shown that Ag_n ($n = 2–4$) nanoclusters tend to bond physically with graphene in contrast to Pd and Pt [58], while the adsorption energy of the Ag_{13} nanocluster suggests chemical bonding occurs when this cluster is supported by defective graphene [59]. Due to the lack of any systematic study on the electronic structure of Ag clusters deposited on N-doped graphene with high surface area and the importance of this system in ORR [58–60], a detailed perspective is highly needed.

Since standard density functional theory cannot properly describe the physical adsorption of clusters to a surface, we have included the van der Waals correction by means of a DFT-D calculation, where van der Waals interactions [61] are added by a pair-wise force field. We have used DFT-D calculations to shed light on the interaction between an Ag cluster and N-doped graphene (denoted by N-graphene). Previous DFT calculations have shown that Ag_8 clusters are the most stable Ag_n ($n = 2–8$) clusters [62]. Accordingly, this study examines the adsorption of Ag_8 clusters on three types of N-doped graphene with five orientations as well as the electronic properties of these complex systems. In addition, the adsorption of O_2 on supported and unsupported Ag_8 clusters has been studied to predict the activity of Ag_8 clusters in ORR.

Methods

Density functional theory was applied to investigate the adsorption of an Ag_8 cluster on a graphene surface using the Perdew–Burke–Ernzerhof (PBE) [63] functional and projector-augmented-wave (PAW) pseudopotentials [64]. The Quantum Espresso package [65] was utilized to perform all calculations. A graphene surface was modeled by a 7×7 supercell containing 98 carbon atoms. Six carbon atoms were substituted by nitrogen atoms and two carbons were removed from the system to produce defects. The supercell was periodic in the xy plane and a 30 Å vacuum was applied in the z-direction to avoid interactions between periodic images. These structures were fully relaxed until the forces on atoms were reduced below 0.05 eV/Å and the total energy convergence reached 10^{-4} a.u. Electronic structure calculations of Ag_8 deposited on N-doped graphene was performed using a 544 eV kinetic energy cutoff, and a $2 \times 2 \times 1$ Monkhorst–Pack [66] grid of k-points was applied for the sampling of Brillouin zone. The DFT-D approach [61] is used to include weak dispersive interactions. For O_2 adsorption on Ag_8/N-doped graphene, a plane wave cutoff of 1020 eV was employed using the Γ-point.

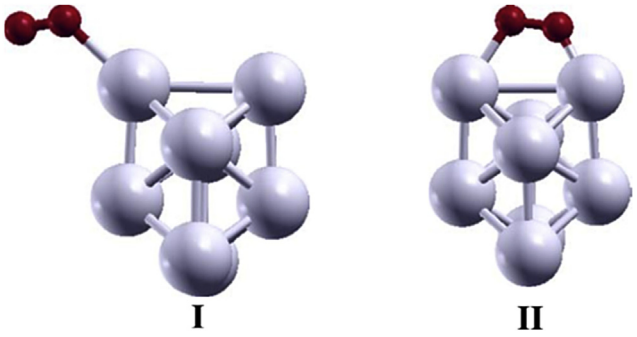

Fig. 1 – Two patterns for O_2 adsorption on an Ag_8 cluster. The red and violet spheres are O and Ag atoms, respectively.

Atomic charges on each of the atoms were calculated by means of Bader charge analysis [67,68]. Molecular structures were created using XCrySDen [69].

The adsorption energy between Ag_8 clusters and N-doped graphene was calculated using the following equation:

$$E_{abs} = E(Ag_8@N/G) - E(N/G) - E(Ag_8) \quad (1)$$

where E (Ag_8@N/G), E (N/G) and E (Ag_8) are the total energies of Ag_8 cluster deposited on N-doped graphene, pristine N-doped graphene and the cluster, respectively. For oxygen adsorption on Ag_8 clusters, a similar equation involving the total energies of Ag_8–O_2@N/G complex, the Ag_8@N/G clusters and a single oxygen molecule was utilized:

$$E_{ads} = E(Ag_8 - O_2@N/G) - E(Ag_8@N/G) - E(O_2) \quad (2)$$

As shown in Fig. 1, two possible patterns for the adsorption of O_2 on Ag_n clusters have been proposed according to a recent study [70]. These are (1) O_2 adsorption on one metal atom, (**I**) and O_2 adsorption on two metal atoms (**II**). O_2 preferentially adsorbs on a top position (pattern **I**) rather than at a bridge site (pattern **II**). So in this study, we have investigated the O_2 adsorption on top positions in the freestanding Ag_8 cluster and the cluster deposited on N-doped graphene.

Results and discussion

Electronic structure of the pristine N-graphene

Three kinds of nitrogen doping have been studied in this work. Graphitic-N_1 (or G-N_1) structures are formed by replacing one carbon atom with a nitrogen atom, while pyrrole-N_1 (P-N_1) and pyridinic-N_3 (P-N_3) are formed by removing one carbon atom and substituting one and three carbon atoms with nitrogen, respectively. Fig. 2 shows a graphene sheet with one P-N_3 (**a**), one P-N_1 (**b**) and two G-N_1 (**c1** and **c2**) substitutions.

The optimized values of the bond lengths are shown in Fig. 2. The C–N bond lengths in P-N_3 have smaller values compared to other N-doped structures. The average C–N bond length in P-N_3 is 1.338 Å, as against the 1.421 Å C–C bond lengths in graphene. Moreover, the values of 1.404, 1.409 and 1.403 Å are determined for P-N_1 (**a**), G-N_1 (**c1**) and (**c2**). Unlike P-N_3 and G-N_1, the three C–N bond lengths in P-N_1 are very different, which is due to the lower symmetry around the nitrogen atom. Since the two G-N_1 substitutions (**c1** and **c2**) have different bonding environments, they have slightly different C–N bond lengths. The presented results are in acceptable agreement with the findings of Jiang and Zhou [71], who showed that the C–N bond lengths of P-N_3, P-N_1 and G-N_1 are 1.338, 1.405 and 1.411 Å. In the following sections, only the **c1** position G-N_1 properties will be discussed. The results for the **c2** position, which are very similar, have been included in the supplementary information.

In order to compare the reactivities of different N-doped regions in an N-graphene sheet, the partial density of state

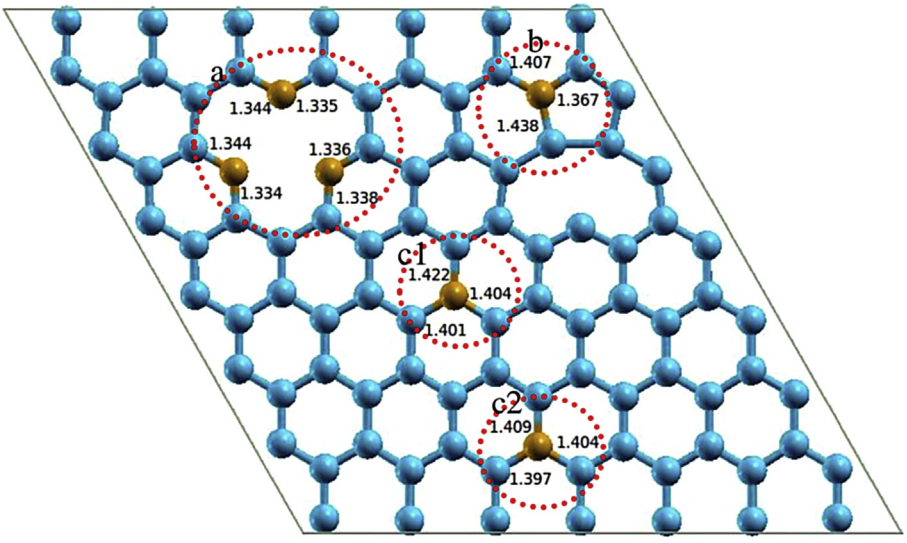

Fig. 2 – Optimized structure of the N-graphene sheet containing pyridinic-N_3 (a), pyrrole-N_1 (b) and graphitic-N_1 (c1 and c2) doping. N–C bond lengths (Å) are also shown. The blue and orange spheres are C and N atoms, respectively. (For interpretation of the references to colour in this figure legend, the reader is referred to the web version of this article.)

(PDOS) plots can be used. In Fig. 3 the total densities of states for N-graphene, along with the PDOS plots for the nitrogen atoms and the carbon atoms bound to them in different N-doped regions of N-graphene are shown. As is evident in Fig. 3a, the Fermi level touches the conduction band and the system has a metallic character whose major contribution comes from the P-N_3 region. From Fig. 3, based on the peak in the PDOS just below the Fermi level, we can infer that the P-N_3 position acts a role as the best active site to stabilize the Ag_8 cluster.

Adsorption of Ag_8 cluster on N-graphene

According to the previous studies [72,73], the Ag_8 cluster has two stable structures with D_{2d} and T_d symmetries in the gas phase. Here, we have used an Ag_8 cluster with D_{2d} symmetry due to its higher chemical activity [74]. Among different possible orientations for the adsorption of Ag_8 cluster on the sheet, we have chosen to study the adsorption via an atom in the vertex position. We have examined the parallel adsorption of the Ag_8 cluster as another possible orientation of the Ag_8 cluster on pyridinic-N_3, where Ag_8 approaches the surface via a square face. The structures obtained for the adsorption of the Ag_8 cluster on N-graphene surface are shown in Fig. 4. Bond lengths, adsorption energies, and the amount of charge transferred are presented in Table 1, which shows that among different possible N-doping positions, P-N_3 exhibits a high adsorption energy and is the most stable position, which is consistent with the results of the previous section.

According to Table 1, the Ag_8 cluster preferentially adsorbs on P-N_3 with an apex Ag atom (P-N_{3a}) with adsorption energy of −7.62 eV. Next place is occupied by parallel adsorption of Ag_8 cluster (P-N_{3b}) with the adsorption energy of 0.16 eV, where it is less stable relative to the apex adsorption. In addition, Ag–N bond lengths in P-N_{3a} are shorter than in P-N_{3b}. Interestingly, the difference between the minimum and maximum Ag–Ag bond lengths in P-N_{3a} (0.52 Å) is higher than P-N_{3b} (0.32 Å), P-N_1 (0.29 Å), G-N_1 (**c1**) (0.32 Å) and bare Ag_8 cluster (0.15 Å). Furthermore, the Ag–N and Ag–C bond lengths decrease with increasing the adsorption energy. Thus P-N_{3a}, which has the highest adsorption energy, also has the shortest Ag–surface bond length (2.323 Å) among all Ag–N and Ag–C bonds. Owing to the presence of a vacancy and three nitrogen atoms, the Ag_8 cluster adsorbs strongly on this active site. Existing nitrogen atoms make neighboring carbon atoms active to absorb Ag atoms. Bader charge values for Ag,

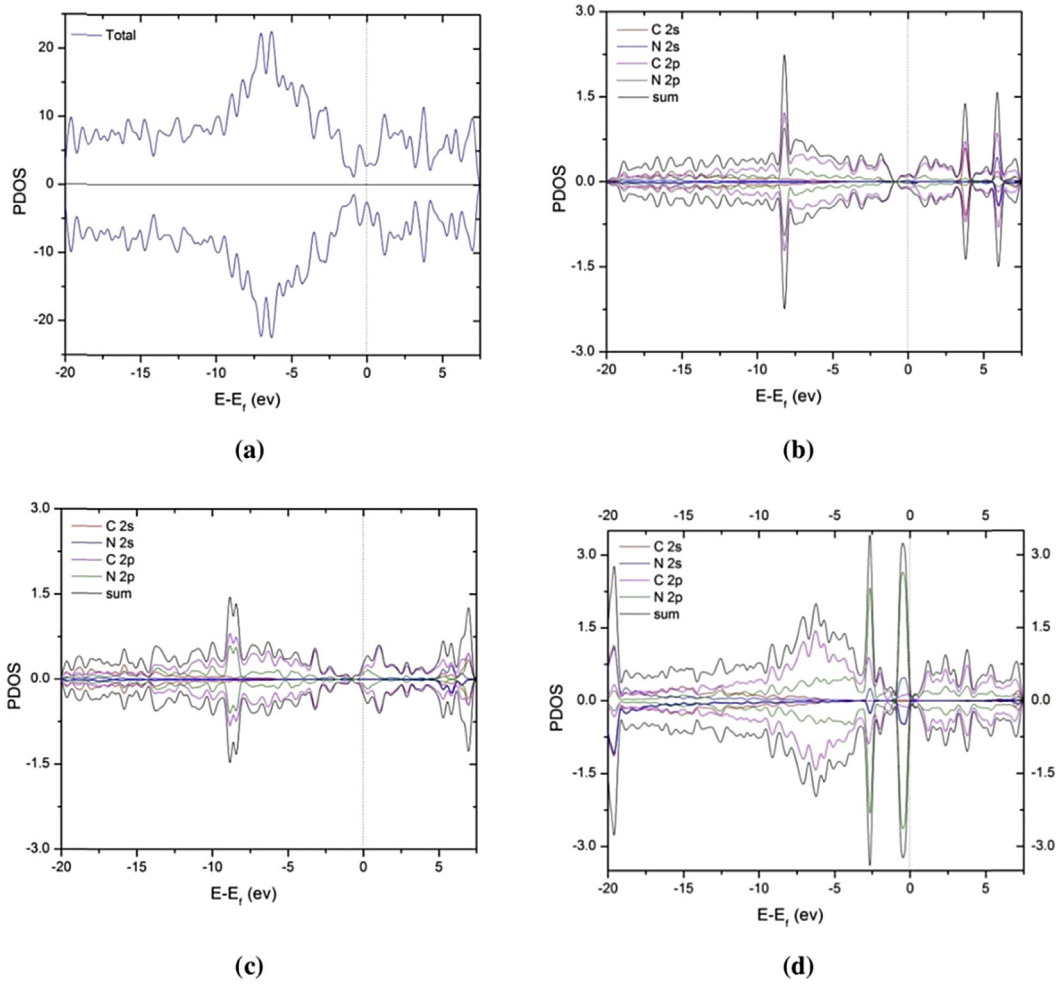

Fig. 3 – Total density of states for the N-graphene (a) along with the partial densities of states for N atoms and the carbon atoms bound to them in the region of (b) P-N_1, (c) G-N_1 (c1) and (d) P-N_3. The Fermi level is set at zero energy.

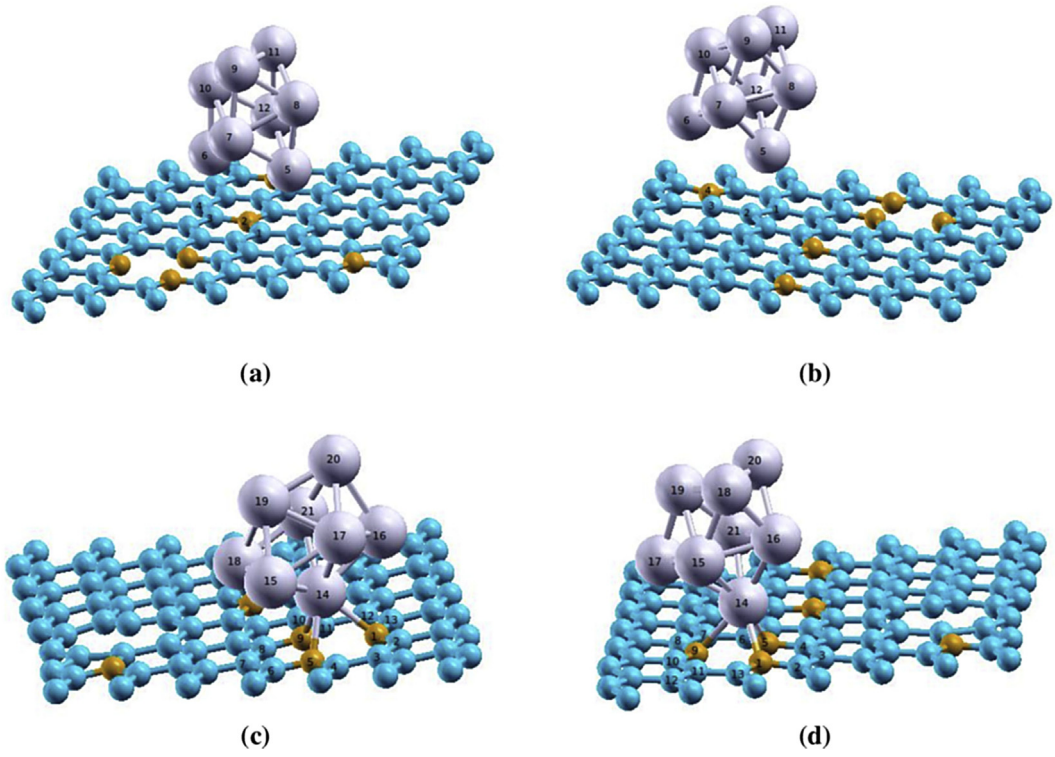

Fig. 4 – Optimized structures of Ag_8 cluster on (a) G-N_1 (c1), (b) P-N_1, (c) P-N_{3b} and (d) P-N_{3a} sites. The blue, orange and violet spheres are C, N and Ag atoms, respectively. (For interpretation of the references to colour in this figure legend, the reader is referred to the web version of this article.)

Table 1 – Adsorption energies, bond lengths (Å) and Bader charges (a.u.) on atoms. a, b denote two different orientation of Ag_8 on P-N_3 according to Fig. 4c and d. The Ag atoms involved in chemical bonds with the surface are denoted by*.

Substrate	E_{ads} (eV)	d_{Ag-C}	d_{Ag-N}	d_{Ag-Ag} (min/max)	Q			
P-N_{3a}	−7.62		2.323	2.748/3.270	N_9	N_5	N_1	Ag_{14}*
			2.464					
			2.366		−2.77	−2.76	−2.73	0.34
P-N_{3b}	−7.46		2.420	2.739/3.060	N_9	N_1	N_5	Ag_{14}*
			2.431					
			2.442		−2.76	−2.74	−2.77	0.35
P-N_1	−6.90	2.540		2.695/2.986		C_2	C_1	Ag_5*
		2.663				−0.10	0.03	0.11
G-N_1 (c1)	−6.89	2.648		2.709/3.029	Ag_6*	C_4	C_1	Ag_5*
		2.754			0.08	−0.02	0.86	0.06

C, and N atoms involved in bonds are listed in Table 1. Negative and positive signs show electron gain and loss, respectively. In P-N_{3a}, nitrogen atoms have higher electronic density due to the more electrophilic character of nitrogen atoms compared to carbon atoms. As a result, nitrogen atoms with the help of carbon atoms can increase the adsorption interaction with the inert cluster of Ag_8. As shown in Fig. 5, Bader charges on Ag atoms next to the surface are clearly correlated with the adsorption energies of the Ag_8 cluster on the N-graphene surface.

To further investigate the binding mechanism of the cluster supported surface, we have calculated the PDOS plots, which are shown in Fig. 6. As can be inferred in Fig. 6a, the valence band of P-N_{3a} consists mainly of the *p* orbitals of nitrogen atoms and *d* orbitals of silver atoms while the conduction band is primarily composed of *p* orbitals of nitrogen atoms. The same trend occurs in P-N_{3b} according to Fig. 6b. In P-N_{3a}, the PDOS has a maximal peak at −2.49 eV; the corresponding peak of *d* orbitals and *p* orbitals is at −1.02 eV, but the corresponding peaks in P-N_{3b} occur at −2.59 eV and −1.12 eV, respectively. It is evident that P-N_{3b} peaks occur at lower energies (more negative) relative to the Fermi energy. The PDOS of nitrogen atoms before the adsorption of the silver cluster is shown in Fig. 3d. The corresponding peak for p orbitals of nitrogen atoms appears near the Fermi level at −0.5 eV. After adsorption of silver atoms, these peaks shift to lower energies and interact with the *d* orbitals of silver atoms from −0.5 eV to −5 eV in the valence band. In the case of the G-

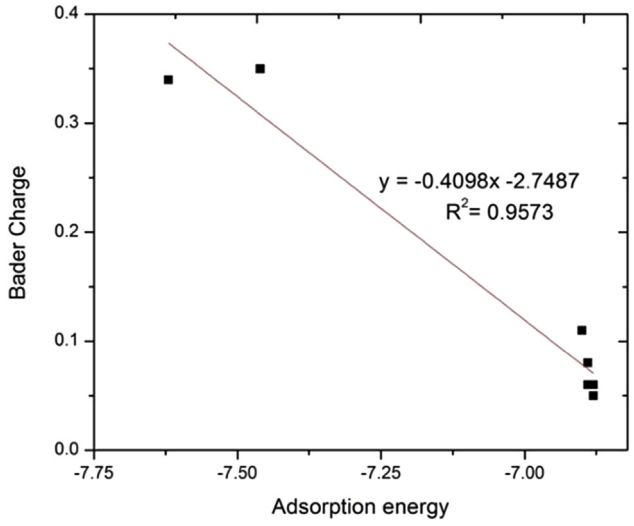

Fig. 5 – Adsorption energy of Ag_8 cluster on the surface as a function of Bader charges of the Ag atom next to the surface.

N_1 (**c1**) substrate, the *d* orbitals of silver atoms interact weakly with the *p* orbitals of carbon atoms (Fig. 6c). In fact, the DOS of the *p* orbitals of carbon atoms in the presence of the cluster reveals similarity to that of the cluster-free surface (Fig. 3c). For the P-N_1 case (Fig. 6d), *d* orbitals strongly interact with the *p* orbitals in comparison to **c1** (Fig. 6c) and **c2** (Fig. S1b) positions in G-N_1 case but pale in comparison to those interactions in P-N_{3a} and P-N_{3b}. Slight differences of DOS for the *p* orbitals of carbon atoms in P-N_1 before (Fig. 3b) and after cluster adsorption compared to P-N_{3a} and P-N_{3b} provide further support for the claim that interactions of the cluster with the surface in P-N_{3a} and P-N_{3b} are stronger than in the P-N_1 structure. The findings shown in Fig. 6 are remarkably consistent with the adsorption energy trends reported in Table 1.

We now study the electrochemical behavior of these Ag_8 clusters with a simple descriptor, i.e., the *d*-band center to predict the ORR activity [75]. In the following, we will focus on the *d*-band center shift. To this end, we have calculated *d*-band center values in two different situations: first, where the Ag_8 cluster is unsupported, and second, where the Ag_8 cluster is adsorbed on N-graphene via one or two silver atoms. According to Fig. 7a, the Ag_8 cluster has two kinds of silver atoms. These two groups are depicted as olive and violet

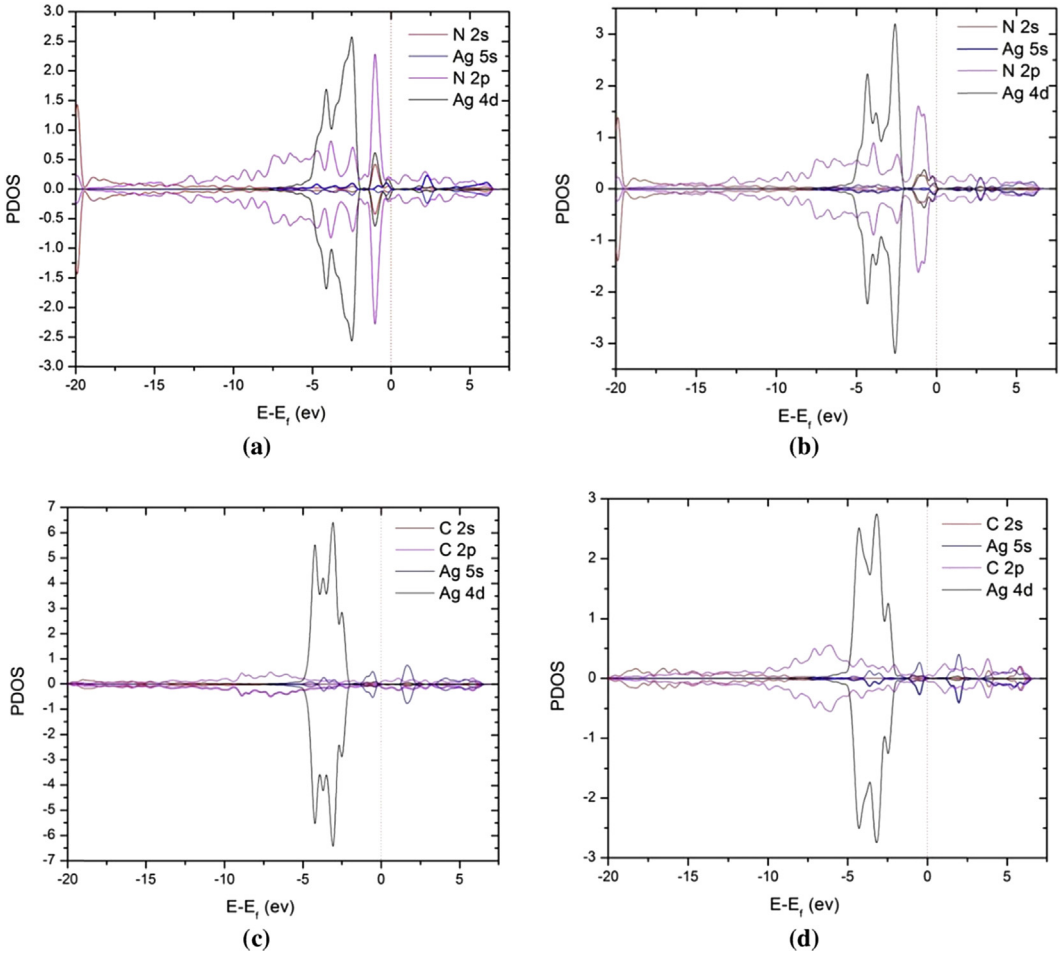

Fig. 6 – PDOS diagrams for Ag, N and C atoms contributing in the binding of Ag_8 cluster for (a) P-N_{3a}, (b) P-N_{3b}, (c) G-N_1 (c1) and (d) P-N_1 cases. The Fermi level is set at zero energy.

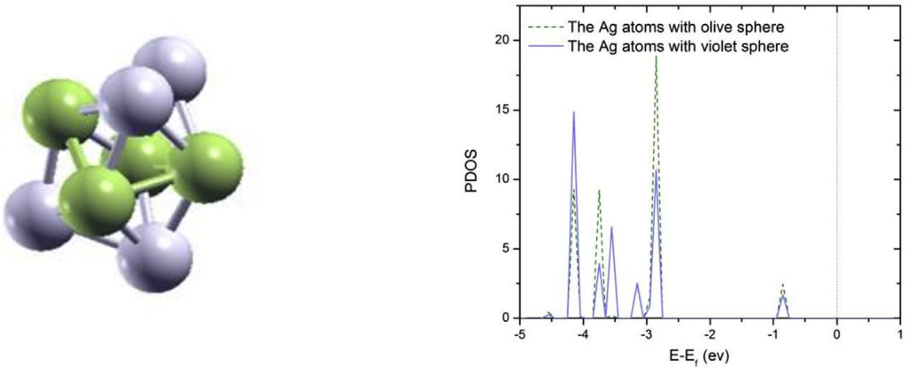

Fig. 7 – (a) An Ag_8 cluster showing two kinds of silver atoms; (b) PDOS diagram for the *d* orbitals of both Ag atom types. Two kinds of Ag atoms are shown in olive and violet.

spheres. In addition, the PDOS diagram of Ag_8 cluster is shown in Fig. 7b for both types of the silver atoms. Here, we have analyzed the *d*-band center for the supported and unsupported Ag_8 clusters. All findings are presented in Table 2. According to the results, the *d*-band center of the adsorbed silver atom on P-N_{3a} shifts to higher energy (more positive) after adsorbing onto the surface; however, the *d*-band center of the adsorbed silver atom at other positions (P-N_{3b}, P-N_1 and G-N_1 (**c1**)) shifts to lower energies (more negative) relative to the gas phase states. Among the cases that show a downshift, there is a slight downshift in P-N_{3b} and G-N_1 (**c1**) cases. In addition to the *d*-band center of adsorbed silver atom presented in Table 2, the *d*-band center for all atoms of the cluster are calculated and the findings indicate that P-N_{3a} has the highest up-shift, with a value of −3.19 eV compared to the unsupported cluster (−3.32 eV). The *d*-band center of the cluster on P-N_{3b}, G-N_1 (**c1**), and P-N_1 are −3.33, −3.25, and −3.22 respectively. Among these cases, the *d*-band center of P-N_1 exhibits the highest up-shift from the Fermi level. It appears that compared to other positions, adsorption of the Ag_8 cluster on P-N_{3a} acts as the reactive position for the ORR reaction. Interestingly, the minimum distance between silver atoms in the Ag_8 cluster is strongly correlated to the *d*-band center of the adsorbed atom (Fig. 8), but is poorly correlated with the *d*-band center of the whole Ag_8 cluster.

The challenge of how to design an optimal catalyst for oxygen reduction reaction still remains: For efficient ORR catalysis, the catalyst should bind molecular oxygen strongly enough to facilitate charge transfer while not blocking the surface. To examine the efficiency of O_2 adsorption on supported complexes, we focus on the adsorption of molecular oxygen on the P-N_{3a} and Ag_8 cluster complex since this complex is particularly stable and the *d*-band center of the complex is close to the Fermi level which leads to high reactivity of supported Ag_8 cluster.

Table 2 – *d*-Band center before and after adsorption and the energy shift (in eV) for the adsorbed Ag atom of an Ag_8 cluster.

Substrate	ε_d (before)	ε_d (after)	$\Delta\varepsilon_d$
P-N_{3a}	−3.44	−3.16	0.28
P-N_{3b}	−3.21	−3.24	−0.03
P-N_1	−3.44	−3.54	−0.10
G-N_1 (**c1**)	−3.44	−3.46	−0.02

Adsorption of molecular oxygen on supported and unsupported Ag_8 clusters

In this section we examine the adsorption of O_2 molecules on Ag_8 clusters. In Fig. 9a the minimum energy structure of molecular oxygen adsorbed on an unsupported Ag_8 cluster is shown. The adsorption energies, defined as the energy difference between the cluster complex with bound molecular oxygen and its components, the Ag–O and O–O bond distances as well as Bader charge analyses for the adsorption on different Ag atoms are listed in Table 3. In a previous study it was found that a Pauling-conformation is greatly favored for O_2 adsorption [70], hence this type of O_2 adsorption on different atoms of the Ag_8 cluster was studied.

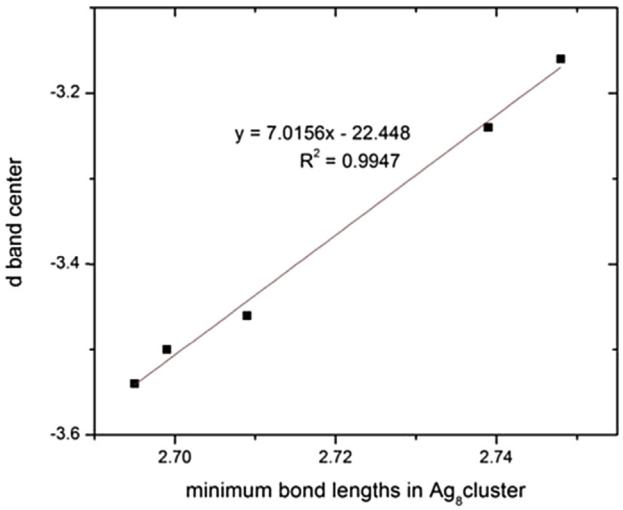

Fig. 8 – *d*-Band center of the adsorbed Ag atom as a function of the minimum Ag–Ag bond length for adsorbed Ag_8 clusters.

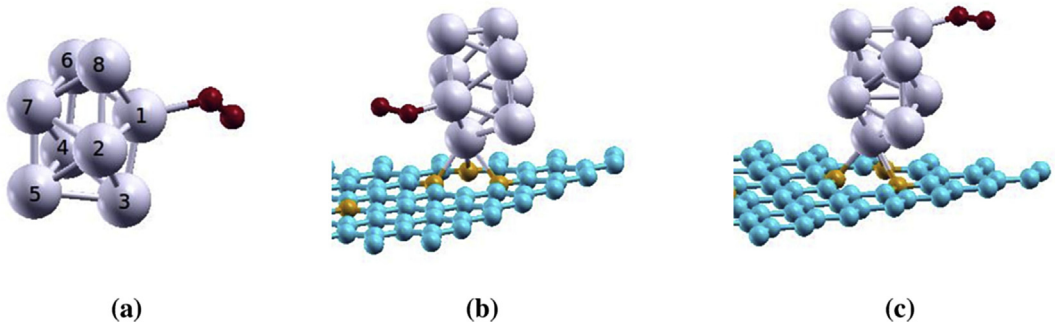

Fig. 9 – Optimized structures of (a) Ag_8O_2 (b) adsorption of O_2 on Ag (2) supported (c) adsorption of O_2 on Ag (6) supported. The blue, orange, violet and red spheres are C, N, Ag and O atoms, respectively. (For interpretation of the references to colour in this figure legend, the reader is referred to the web version of this article.)

According to the calculated adsorption energies listed in Table 3, the adsorption of O_2 on all of the atoms of the Ag_8 cluster is exothermic. Therefore, all adsorption positions could be suitable positions for ORR. However, O–O bond lengths play an important role in determining the catalytic activity of the complex in ORR: Elongation of O–O bond lengths relative to the gas phase value (found here to be 1.231 Å) can facilitate breaking of the O–O bond in the ORR mechanism. Moreover, prior to breaking the oxygen–oxygen bond, O_2 molecules adsorb on metal atoms in the cluster and the bond elongation is related to the ability of Ag atoms to transfer electrons to O_2. In addition, our DFT-D (GGA-PBE) adsorption energy results are different with those reported by Liao and coworkers [70] who investigated adsorption energies of O_2 on Ag_n clusters by DFT (BP86 [76,77] (0.07 eV), revPBE [78] (−0.05 eV) and B3LYP [79,80] (−0.14 eV)) calculations without any van der Waals correction.

As mentioned in the previous section, we can classify Ag_8 cluster atoms into two groups (Fig. 7). Silver atoms 1, 2, 4, and 7 are in the first group and the remaining atoms are in the second group (Fig. 9a). Since all atoms within a group are treated similarly, the effect of support on the adsorption energies of O_2 on silver atoms 2 and 6 were considered. In Fig. 9b and c, the optimized structures are shown for the adsorption of oxygen on a supported Ag_8 cluster. The corresponding properties are reported in Table 4.

As Table 4 shows, the adsorption of O_2 on the Ag_8@N–-graphene complex is exothermic for both positions. The adsorption energies are more positive and the O–O bond elongation is greater than for those in an unsupported cluster. We can compare our data with published findings on Pt (111) as an electrocatalyst with high kinetic capability for ORR. According to previous studies, the adsorption energy of O_2 on Pt (111) was reported to be between −0.43 and −0.72 for different positions on Pt (111) [81,82] by using DFT (PBE-GGA). But the present O–O distances (1.277 Å) are shorter than those on the Pt (111) surface (1.35 Å with adsorption energy of −0.65 eV). Utilizing DFT-D (GGA-PW91) calculations, Yan and coworkers [83] examined oxygen adsorption on transition metal surfaces. The presented results in Table 4 are same as the reported value of Mulliken charge of adsorbed O_2 (−0.26 a.u.) on Pt (111) by them, however, the adsorption energy (−0.60 eV) and O_2 bond length (1.36 Å) is somehow different. On the other hand, their results for Ag (111) are totally different to our results with adsorption energy, bond length and charge of +0.19 eV, 1.35 Å and −0.43 a.u., respectively. So, it is clear that more similar characters exist between supported Ag_8 cluster and Pt (111) when adsorbing O_2 than Ag (111). However, a general agreement exists between our data and Ag (110) results reported by Loncaric and coworkers [84] (and Roy and coworkers [85]) who conducted their studies with DFT (PBE-GGA) calculations and projector-Augmented-Wave (PAW) pseudopotentials [64], like our calculations. The values reported by them are −0.33 eV (−0.27 eV), 2.20 Å (2.15 Å) and 1.31 Å (1.31 Å) for adsorption energy, Ag–O distance and O_2 bond length, respectively.

Now regarding the positions of the *d*-band center, it is clear that there is no correlation between the *d*-band center and adsorption energy. In other words, as previous studies indicate [86,87], the shift of the *d*-band center to lower energies (or more negative energies) does not cause weaker bonding in the adsorption of some cases such as O_2. All O–O adsorption energy and bond length data suggest that a supported Ag_8 cluster is a better catalyst than an unsupported Ag_8 cluster. This is because an ORR catalyst should not adsorb O_2 so strongly that O_2 molecules block the catalyst surface. Finally, the key question is what leads to the elongation of bonds here?

As can be seen in Table 4, the chemisorption of O_2 on the cluster leads to electron transfer from the silver atom to the O_2 molecule. The Ag atom that is involved in bonding with the O atom loses 0.02e and 0.118e, and O_2 molecules gain 0.105e and 0.065e and reach to final charges of −0.281 and −0.257,

Table 3 – Calculated properties for O_2 adsorption on an unsupported Ag_8 cluster. *n* is the label of silver atoms which bind to the O_2 molecule.

n	E_{ads} (eV)	d_{Ag-O} (Å)	d_{O-O} (Å)	Q $_{O_2}$
1	−0.88	2.365	1.266	
2	−0.85	2.440	1.263	−0.176
3	−0.92	2.307	1.269	
4	−0.87	2.387	1.267	
5	−0.92	2.302	1.270	
6	−0.92	2.301	1.269	−0.192
7	−0.87	2.380	1.266	
8	−0.91	2.302	1.270	

Table 4 – Adsorption energies (eV), bond lengths (Å), Bader charges (a.u.) and *d*-band center (eV) for the adsorption of O_2 on two different silver atoms ($n = 2$ and 6) of an Ag_8 complex adsorbed at a P-N_{3a} position of N-graphene. The Ag atom involved in chemical bonds with the surface is denoted by*. The values in parentheses are for the unsupported cluster.

n	E_{ads}	d_{Ag-O}	d_{O-O}	Q_{Ag^*}	Q_{O_2}	ε_d
2	−0.39	2.327	1.277	0.205 (0.185)	−0.281	−3.19 (−3.21)
6	−0.32	2.283	1.277	0.339 (0.221)	−0.257	−3.18 (−3.44)

respectively. In addition, the same trend is seen in the N-graphene where the Ag atom has a more positive charge than before the adsorption of O_2. In Fig. 10, the PDOS plots of adsorbed O_2 on supported clusters are presented. O_2 $2\pi^*$ orbitals with spin down and up are located above and below the Fermi level between 1 and −2 eV. On the other hand, O_2 2π orbitals are placed between −5 and −8 eV and *d* and *p* orbitals do not show any peaks, as shown in Fig. 10. The position of silver *d* orbitals is between −2.5 and −5.5 eV, exactly in the middle of the O_2 $2\pi^*$ and 2π peaks. So, electrons can transfer from *d* orbitals to O_2 $2\pi^*$ orbitals, and these transfers can cause the elongation of the O_2 bond due to the position of the transferred electrons placed in $2\pi^*$ orbitals.

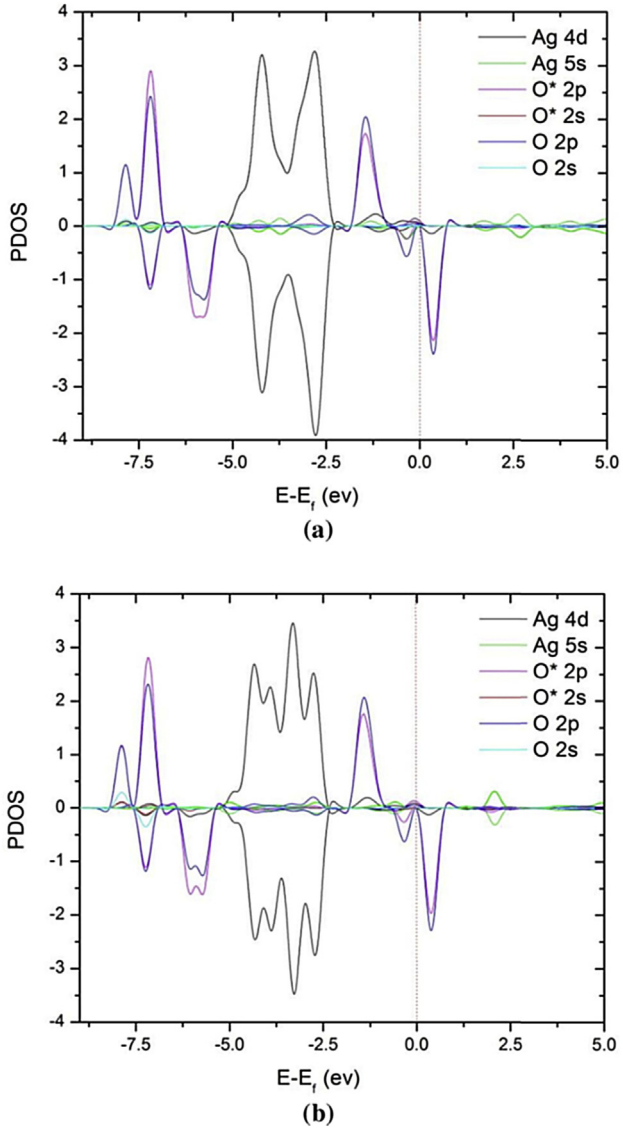

Fig. 10 – PDOS diagrams for (a) O_2 adsorbed on Ag_8 (2) supported cluster (b) O_2 adsorbed on Ag_8 (6) supported cluster.

Conclusions

In summary, this study examines the properties of N-doped graphene as a support for the catalytic reactivity of Ag_8 towards ORR via DFT-D calculations. Adsorption energies of the Ag_8 cluster on three types of N-doped graphene with five orientations were calculated. Among these orientations, the adsorption energy of the Ag_8 cluster with a vertex atom in the P-N_3 position (P-N_{3a} orientation) is the most stable with an adsorption energy of −7.62 eV. These adsorption energies are correlated with Bader charge analyses, which show that an Ag atom adsorbed on the P-N_3 position has a greater positive charge than the other positions. PDOS findings are in general agreement with Bader charge and adsorption energies. The results indicate that a strong correlation exists between the *d*-band center of adsorbed Ag atoms and minimum Ag–Ag bond lengths in the cluster as well as between the adsorption energies of the cluster and Bader charges of the Ag atoms nearest to the surface. The *d*-band center results, as well as adsorption energies, indicate that P-N_{3a} may be the most favorable site to interact with O_2 molecules. All the data show that there is no relationship between *d*-band center positions and adsorption energies of O_2 on the supported cluster. Investigation of O_2 adsorption on the supported cluster indicates that the presence of a support can improve the catalytic activity of a complex.

Appendix A. Supplementary data

Supplementary data related to this article can be found at http://dx.doi.org/10.1016/j.ijhydene.2017.04.238.

REFERENCES

[1] Jaouen F, Proietti E, Lefèvre M, Chenitz R, Dodelet JP, Wu G, et al. Recent advances in non-precious metal catalysis for oxygen-reduction reaction in polymer electrolyte fuel cells. Energy Environ Sci 2011;4(1):114–30.
[2] Katsounaros I, Cherevko S, Zeradjanin AR, Mayrhofer KJ. Oxygen electrochemistry as a cornerstone for sustainable energy conversion. Angew Chem Int Ed 2014;53(1):102–21.
[3] Liew KB, Daud WR, Ghasemi M, Leong JX, Lim SS, Ismail M. Non-Pt catalyst as oxygen reduction reaction in microbial fuel cells: a review. Int J Hydrogen Energy 2014;39(10):4870–83.

[4] Li R, Wei Z, Gou X. Nitrogen and phosphorus dual-doped graphene/carbon nanosheets as bifunctional electrocatalysts for oxygen reduction and evolution. ACS Catal 2015;5(7):4133–42.
[5] Trogadas P, Fuller TF, Strasser P. Carbon as catalyst and support for electrochemical energy conversion. Carbon 2014;75:5–42.
[6] Hussain S, Erikson H, Kongi N, Merisalu M, Ritslaid P, Sammelselg V, et al. Heat-treatment effects on the ORR activity of Pt nanoparticles deposited on multi-walled carbon nanotubes using magnetron sputtering technique. Int J Hydrogen Energy 2017;42(9):5958–70.
[7] Bharti A, Cheruvally G, Muliankeezhu S. Microwave assisted facile synthesis of Pt/CNT catalyst for proton exchange membrane fuel cell application. Int J Hydrogen Energy 2017;42(16):11622–31.
[8] Cheng N, Liu J, Banis MN, Geng D, Li R, Ye S, et al. High stability and activity of Pt electrocatalyst on atomic layer deposited metal oxide/nitrogen-doped graphene hybrid support. Int J Hydrogen Energy 2014;39(28):15967–74.
[9] Puthusseri D, Ramaprabhu S. Oxygen reduction reaction activity of platinum nanoparticles decorated nitrogen doped carbon in proton exchange membrane fuel cell under real operating conditions. Int J Hydrogen Energy 2016;41(30):13163–70.
[10] Bhowmik T, Kundu MK, Barman S. Highly active and durable Pd nanoparticles-porous graphitic carbon nitride composite for electrocatalytic oxygen reduction reaction. Int J Hydrogen Energy 2016;41(33):14768–77.
[11] Xue YH, Zhang L, Zhou WJ, Chan SH. Pd nanoparticles supported on PDDA-functionalized carbon black with enhanced ORR activity in alkaline medium. Int J Hydrogen Energy 2014;39(16):8449–56.
[12] Proietti E, Jaouen F, Lefèvre M, Larouche N, Tian J, Herranz J, et al. Iron-based cathode catalyst with enhanced power density in polymer electrolyte membrane fuel cells. Nat Commun 2011;2:416-1–416-9.
[13] Yang W, Liu X, Yue X, Jia J, Guo S. Bamboo-like carbon nanotube/Fe_3C nanoparticle hybrids and their highly efficient catalysis for oxygen reduction. J Am Chem Soc 2015;137(4):1436–9.
[14] Ding W, Li L, Xiong K, Wang Y, Li W, Nie Y, et al. Shape fixing via salt recrystallization: a morphology-controlled approach to convert nanostructured polymer to carbon nanomaterial as a highly active catalyst for oxygen reduction reaction. J Am Chem Soc 2015;137(16):5414–20.
[15] Hu Y, Jensen JO, Zhang W, Cleemann LN, Xing W, Bjerrum NJ, et al. Hollow spheres of iron carbide nanoparticles encased in graphitic layers as oxygen reduction catalysts. Angew Chem Int Ed 2014;53(14):3675–9.
[16] Jiang WJ, Gu L, Li L, Zhang Y, Zhang X, Zhang LJ, et al. Understanding the high activity of Fe-NC electrocatalysts in oxygen reduction: Fe/Fe_3C nanoparticles boost the activity of $Fe-N_x$. J Am Chem Soc 2016;138:3570–8.
[17] Lim EJ, Choi SM, Seo MH, Kim Y, Lee S, Kim WB. Highly dispersed Ag nanoparticles on nanosheets of reduced graphene oxide for oxygen reduction reaction in alkaline media. Electrochem Commun 2013;28:100–3.
[18] Wang Z, Xin L, Zhao X, Qiu Y, Zhang Z, Baturina OA, et al. Carbon supported Ag nanoparticles with different particle size as cathode catalysts for anion exchange membrane direct glycerol fuel cells. Renew Energy 2014;62:556–62.
[19] Lim DH, Wilcox J. DFT-based study on oxygen adsorption on defective graphene-supported Pt nanoparticles. J Phys Chem C 2011;115(46):22742–7.
[20] Tian Y, Liu YJ, Zhao JX, Ding YH. High stability and superior catalytic reactivity of nitrogen-doped graphene supporting Pt nanoparticles as a catalyst for the oxygen reduction reaction: a density functional theory study. RSC Adv 2015;5(43):34070–7.
[21] Xu D, Liu YJ, Zhao JX, Cai QH, Wang XZ. Theoretical study of the deposition of Pt clusters on defective hexagonal boron nitride (h-BN) sheets: morphologies, electronic structures, and interactions with O. J Phys Chem C 2014;118(17):8868–76.
[22] Xia M, Ding W, Xiong K, Li L, Qi X, Chen S, et al. Anchoring effect of exfoliated-montmorillonite-supported Pd catalyst for the oxygen reduction reaction. J Phys Chem 2013;117(20):10581–8.
[23] Ding W, Xia MR, Wei ZD, Chen SG, Hu JS, Wan LJ, et al. Enhanced stability and activity with Pd–O junction formation and electronic structure modification of palladium nanoparticles supported on exfoliated montmorillonite for the oxygen reduction reaction. Chem Commun 2014;50(50):6660–3.
[24] Kong XK, Chen CL, Chen QW. Doped graphene for metal-free catalysis. Chem Soc Rev 2014;43(8):2841–57.
[25] Jiang DE, Cooper VR, Dai S. Porous graphene as the ultimate membrane for gas separation. Nano Lett 2009;9(12):4019–24.
[26] Feng YY, Liu ZH, Kong WQ, Yin QY, Du LX. Promotion of palladium catalysis by silver for ethanol electro-oxidation in alkaline electrolyte. Int J Hydrogen Energy 2014;39(6):2497–504.
[27] Yasmin S, Ahmed MS, Jeon S. A noble silver nanoflower on nitrogen doped carbon nanotube for enhanced oxygen reduction reaction. Int J Hydrogen Energy 2017;42(2):1075–84.
[28] Jiang R, Moton E, McClure JP, Bowers Z. A highly active and alcohol-tolerant cathode electrocatalyst containing Ag nanoparticles supported on graphene. Electrochim Acta 2014;127:146–52.
[29] Fazil A, Chetty R. Synthesis and evaluation of carbon nanotubes supported silver catalyst for alkaline fuel cell. Electroanalysis 2014;26(11):2380–7.
[30] Xu L, Li H, Xia J, Wang L, Xu H, Ji H, et al. Graphitic carbon nitride nanosheet supported high loading silver nanoparticle catalysts for the oxygen reduction reaction. Mater Lett 2014;128:349–53.
[31] Soo LT, Loh KS, Mohamad AB, Daud WR, Wong WY. Synthesis of silver/nitrogen-doped reduced graphene oxide through a one-step thermal solid-state reaction for oxygen reduction in an alkaline medium. J Power Sources 2016;324:412–20.
[32] Narayanamoorthy B, Panneerselvam N, Sita C, Pasupathi S, Balaji S, Moon IS. Enhanced stabilities of Ag electrocatalyst as self-standing and multiwalled carbon nanotube supported nanostructures for oxygen reduction in alkaline medium. J Electrochem Soc 2016;163(5):H313–20.
[33] Jin S, Chen M, Dong H, He B, Lu H, Su L, et al. Stable silver nanoclusters electrochemically deposited on nitrogen-doped graphene as efficient electrocatalyst for oxygen reduction reaction. J Power Sources 2015;274:1173–9.
[34] Mayavan S, Sim JB, Choi SM. Easy synthesis of nitrogen-doped graphene–silver nanoparticle hybrids by thermal treatment of graphite oxide with glycine and silver nitrate. Carbon 2012;50(14):5148–55.
[35] Yu D, Yao J, Qiu L, Wu Y, Li L, Feng Y, et al. The synergetic effect of N-doped graphene and silver nanowires for high electrocatalytic performance in the oxygen reduction reaction. RSC Adv 2013;3(29):11552–5.
[36] Appleby AJ. Oxygen reduction and corrosion kinetics on phase-oxide-free palladium and silver electrodes as a function of temperature in 85% orthophosphoric acid. J Electrochem Soc 1970;117(11):1373–8.
[37] Blizanac BB, Ross PN, Markovic NM. Oxygen electroreduction on Ag (111): the pH effect. Electrochim Acta 2007;52(6):2264–71.

[38] Blizanac BB, Ross PN, Marković NM. Oxygen reduction on silver low-index single-crystal surfaces in alkaline solution: rotating ring DiskAg (hkl) studies. J Phys Chem B 2006;110(10):4735–41.
[39] Neumann CC, Laborda E, Tschulik K, Ward KR, Compton RG. Performance of silver nanoparticles in the catalysis of the oxygen reduction reaction in neutral media: efficiency limitation due to hydrogen peroxide escape. Nano Res 2013;6(7):511–24.
[40] Lee K, Ahmed MS, Jeon S. Various carbon chain containing linkages grafted graphene with silver nanoparticles electrocatalysts for oxygen reduction reaction. J Electrochem Soc 2015;162(1):F1–8.
[41] Lima FH, Zhang J, Shao MH, Sasaki K, Vukmirovic MB, Ticianelli EA, et al. Catalytic activity–d-band center correlation for the O_2 reduction reaction on platinum in alkaline solutions. J Phys Chem C 2007;111(1):404–10.
[42] Anderson AB. O_2 reduction and CO oxidation at the Pt-electrolyte interface. The role of H_2O and OH adsorption bond strengths. Electrochim Acta 2002;47(22):3759–63.
[43] Nørskov JK, Rossmeisl J, Logadottir A, Lindqvist LR, Kitchin JR, Bligaard T, et al. Origin of the overpotential for oxygen reduction at a fuel-cell cathode. J Phys Chem B 2004;108(46):17886–92.
[44] Lim DH, Wilcox J. Mechanisms of the oxygen reduction reaction on defective graphene-supported Pt nanoparticles from first-principles. J Phys Chem C 2012;116(5):3653–60.
[45] Casanovas J, Ricart JM, Rubio J, Illas F, Jiménez-Mateos JM. Origin of the large N 1s binding energy in X-ray photoelectron spectra of calcined carbonaceous materials. J Am Chem Soc 1996;118(34):8071–6.
[46] Ouyang W, Zeng D, Yu X, Xie F, Zhang W, Chen J, et al. Exploring the active sites of nitrogen-doped graphene as catalysts for the oxygen reduction reaction. Int J Hydrogen Energy 2014;39(28):15996–6005.
[47] Liu Y, Li J, Li W, Li Y, Zhan F, Tang H, et al. Exploring the nitrogen species of nitrogen doped graphene as electrocatalysts for oxygen reduction reaction in Al–air batteries. Int J Hydrogen Energy 2016;41(24):10354–65.
[48] Guo C, Tong X, Guo XY. Nitrogen-doped mesoporous network-like carbon as an efficient metal-free electrocatalyst for oxygen reduction reaction. Int J Hydrogen Energy 2016;41(48):22941–51.
[49] Lee KR, Lee KU, Lee JW, Ahn BT, Woo SI. Electrochemical oxygen reduction on nitrogen doped graphene sheets in acid media. Electrochem Commun 2010;12(8):1052–5.
[50] Feng L, Yang L, Huang Z, Luo J, Li M, Wang D, et al. Enhancing electrocatalytic oxygen reduction on nitrogen-doped graphene by active sites implantation. Sci Rep 2013;3:3306-1–3306-8.
[51] Wang L, Yin F, Yao C. N-doped graphene as a bifunctional electrocatalyst for oxygen reduction and oxygen evolution reactions in an alkaline electrolyte. Int J Hydrogen Energy 2014;39(28):15913–9.
[52] Huang X, Zhao Y, Ao Z, Wang G. Micelle-template synthesis of nitrogen-doped mesoporous graphene as an efficient metal-free electrocatalyst for hydrogen production. Sci Rep 2014;4:7557-1–7557-6.
[53] Hu T, Sun X, Sun H, Xin G, Shao D, Liu C, et al. Rapid synthesis of nitrogen-doped graphene for a lithium ion battery anode with excellent rate performance and super-long cyclic stability. Phys Chem Chem Phys 2014;16(3):1060–6.
[54] Deng D, Pan X, Yu L, Cui Y, Jiang Y, Qi J, et al. Toward N-doped graphene via solvothermal synthesis. Chem Mater 2011;23(5):1188–93.
[55] Gopalakrishnan K, Govindaraj A, Rao CN. Extraordinary supercapacitor performance of heavily nitrogenated graphene oxide obtained by microwave synthesis. J Mater Chem A 2013;1(26):7563–5.
[56] Shi Z, Kutana A, Yakobson BI. How much N-doping can graphene sustain. J Phys Chem Lett 2015;6(1):106–12.
[57] Zhang Y, Ge J, Wang L, Wang D, Ding F, Tao X, et al. Manageable N-doped graphene for high performance oxygen reduction reaction. Sci Rep 2013;3:2771-1–2771-8.
[58] Del Castillo RM, Sansores LE. Study of the electronic structure of Ag, Au, Pt and Pd clusters adsorption on graphene and their effect on conductivity. Eur Phys J B 2015;88(10):248-1–248-13.
[59] Meeprasert J, Junkaew A, Rungnim C, Kunaseth M, Kungwan N, Promarak V, et al. Capability of defective graphene-supported Pd_{13} and Ag_{13} particles for mercury adsorption. Appl Surf Sci 2016;364:166–75.
[60] Lopes JH, Ye S, Gostick JT, Barralet JE, Merle G. Electrocatalytic oxygen reduction performance of silver nanoparticle decorated electrochemically exfoliated graphene. Langmuir 2015;31(35):9718–27.
[61] Barone V, Casarin M, Forrer D, Pavone M, Sambi M, Vittadini A. Role and effective treatment of dispersive forces in materials: polyethylene and graphite crystals as test cases. J Comput Chem 2009;30(6):934–9.
[62] Alonso JA. Electronic and atomic structure, and magnetism of transition-metal clusters. Chem Rev 2000;100(2):637–78.
[63] Perdew JP, Burke K, Ernzerhof M. Generalized gradient approximation made simple. Phys Rev Lett 1996;77(18):3865–8.
[64] Blöchl PE. Projector augmented-wave method. Phys Rev B 1994;50(24):17953–79.
[65] Giannozzi P, Baroni S, Bonini N, Calandra M, Car R, Cavazzoni C, et al. QUANTUM ESPRESSO: a modular and open-source software project for quantum simulations of materials. J Phys Condens Matter 2009;21(39):395502-1–395502-19.
[66] Monkhorst HJ, Pack JD. Special points for Brillouin-zone integrations. Phys Rev B 1976;13(12):5188–92.
[67] Bader RF, Beddall PM. Virial field relationship for molecular charge distributions and the spatial partitioning of molecular properties. J Chem Phys 1972;56(7):3320–9.
[68] Henkelman G, Arnaldsson A, Jónsson H. A fast and robust algorithm for Bader decomposition of charge density. Comput Mater Sci 2006;36(3):354–60.
[69] Kokalj A. Computer graphics and graphical user interfaces as tools in simulations of matter at the atomic scale. Comput Mater Sci 2003;28(2):155–68.
[70] Liao MS, Watts JD, Huang MJ. Theoretical comparative study of oxygen adsorption on neutral and anionic Ag_n and Au_n clusters (n = 2–25). J Phys Chem C 2014;118(38):21911–27.
[71] Jing Y, Zhou Z. Computational insights into oxygen reduction reaction and initial Li_2O_2 nucleation on pristine and N-Doped graphene in Li–O_2 batteries. ACS Catal 2015;5(7):4309–17.
[72] Pereiro M, Baldomir D. Determination of the lowest-energy structure of Ag_8 from first-principles calculations. Phys Rev A 2005;72(4):045201-1–045201-4.
[73] Harb M, Rabilloud F, Simon D, Rydlo A, Lecoultre S, Conus F, et al. Optical absorption of small silver clusters: Ag_n, (n = 4–22). J Chem Phys 2008;129(19):194108-1–194108-9.
[74] Torbatian Z, Hashemifar SJ, Akbarzadeh H. First-principles insights into interaction of CO, NO, and HCN with Ag_8. J Chem Phys 2014;140(8):084314-1–084314-7.
[75] Hammer B, Nørskov JK. Theoretical surface science and catalysis—calculations and concepts. Adv Catal 2000;45:71–129.
[76] Becke AD. Density-functional exchange-energy approximation with correct asymptotic behavior. Phys Rev A 1988;38(6):3098–100.

[77] Perdew JP. Density-functional approximation for the correlation energy of the inhomogeneous electron gas. Phys Rev B 1986;33(12):8822–4.
[78] Zhang Y, Yang W. Comment on "Generalized gradient approximation made simple". Phys Rev Lett 1998;80(4). 890-1-890-1.
[79] Becke AD. Density-functional thermochemistry. III. The role of exact exchange. J Chem Phys 1993;98(7): 5648–52.
[80] Lee C, Yang W, Parr RG. Development of the Colle-Salvetti correlation-energy formula into a functional of the electron density. Phys Rev B 1988;37(2):785–9.
[81] Eichler A, Hafner J. Molecular precursors in the dissociative adsorption of O_2 on Pt (111). Phys Rev Lett 1997;79(22):4481–4.
[82] Qi L, Yu J, Li J. Coverage dependence and hydroperoxyl-mediated pathway of catalytic water formation on Pt (111) surface. J Chem Phys 2006;125(5):054701-1–054701-8.
[83] Yan M, Huang ZQ, Zhang Y, Chang CR. Trends in water-promoted oxygen dissociation on the transition metal surfaces from first principles. Phys Chem Chem Phys 2017;19:2364–71.
[84] Lončarić I, Alducin M, Juaristi JI. Dissociative dynamics of O_2 on Ag (110). Phys Chem Chem Phys 2015;17(14):9436–45.
[85] Roy S, Mujica V, Ratner MA. Chemistry at molecular junctions: rotation and dissociation of O_2 on the Ag (110) surface induced by a scanning tunneling microscope. J Chem Phys 2013;139(7):074702-1–074702-11.
[86] Hyman MP, Medlin JW. Effects of electronic structure modifications on the adsorption of oxygen reduction reaction intermediates on model Pt (111)-alloy surfaces. J Phys Chem C 2007;111(45):17052–60.
[87] Duan Z, Wang G. A first principles study of oxygen reduction reaction on a Pt (111) surface modified by a subsurface transition metal M (M = Ni, Co, or Fe). Phys Chem Chem Phys 2011;13(45):20178–87.